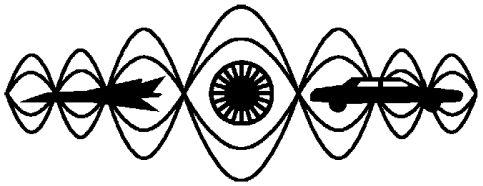

Tenth International Congress
on Sound and Vibration
7-10 July 2003 • Stockholm, Sweden

WHEEL/RAIL ROLLING NOISE - THE EFFECTS OF NON-LINEARITIES IN THE CONTACT ZONE

David Thompson, Tianxing Wu and Tristan Armstrong

Institute of Sound and Vibration Research
University of Southampton, Highfield
Southampton, SO17 1BJ UK
e-mail: djt@isvr.soton.ac.uk

Abstract. Models that have been developed for wheel/rail rolling noise are generally linear in order to make use of a frequency-domain approach. In fact, the local elasticity between the wheel and the rail exhibits a non-linear stiffness behaviour due to geometrical effects. This is, therefore, usually linearised about a nominal static preload. For large defects on the wheel or rail surface, however, such an approach can no longer be used and a time-domain solution including the non-linearities is required. By using simplified models of the wheel and rail dynamics in such a time-stepping model, the effects of the non-linearities have been determined. It has been found that, for normal levels of surface roughness found on wheels and rails, the linear models give a satisfactory prediction. However, for larger defects, such as wheel flats or rail joints, the non-linear effects are found to be significant. A hybrid approach is used to predict the noise radiation due to such defects, for which more detailed dynamic models should be incorporated. The contact force from the non-linear calculation is converted back to an equivalent roughness that can be used in a linear model for the response and noise radiation.

1. INTRODUCTION

When a wheel rolls on a rail, irregularities on the wheel and rail surfaces excite vibrations which radiate noise. Theoretical models describing the interaction between a railway wheel and the track are used for predicting noise generation, as well as wheel and track vibration, fatigue damage and rail corrugation. Often, especially for noise prediction, a linear model is used, which has the advantage that calculations can be carried out in the frequency domain [1,2]. In practice, although the wheel can be considered as a linear system, the local elastic deformation of the contact zone has a

non-linear stiffness characteristic [3], as do the rail pads and the ballast in the track structure [4]. Nevertheless, a linear model is usually justified on the basis that the corresponding deflections are small. This paper reviews recent research that has investigated the effects of the non-linear behaviour of the contact spring on the wheel/rail interaction force and hence on rolling noise for situations where the deflections of the contact spring are no longer small. The frequency range of interest for rolling noise is generally 50 to 5000 Hz.

Time-domain models, incorporating the non-linearities in the contact zone, have been used by, for example, Clark *et al* [5] and Nielsen [6]. These models contain large numbers of degrees of freedom to represent the track. Nevertheless they are limited to a maximum frequency of around 1500 Hz. In the present study, simplified models of the wheel and rail are used in a time-stepping model in order to determine the effects of the non-linearities. Although these models use only a small number of degrees of freedom they are representative for a wide frequency range.

2. THE EFFECT OF NON-LINEARITIES ON ROLLING NOISE

2.1 Wheel/rail interaction

A model for the generation of rolling noise is shown in Figure 1. As the wheel rolls over the rail, the roughness of the rail and wheel surfaces induces a relative motion in the vertical direction. A roughness of wavelength l, traversed at a speed v, induces vibration at the circular frequency $w = 2pv/l$. This is represented in Figure 1 by a static wheel and a moving irregularity.

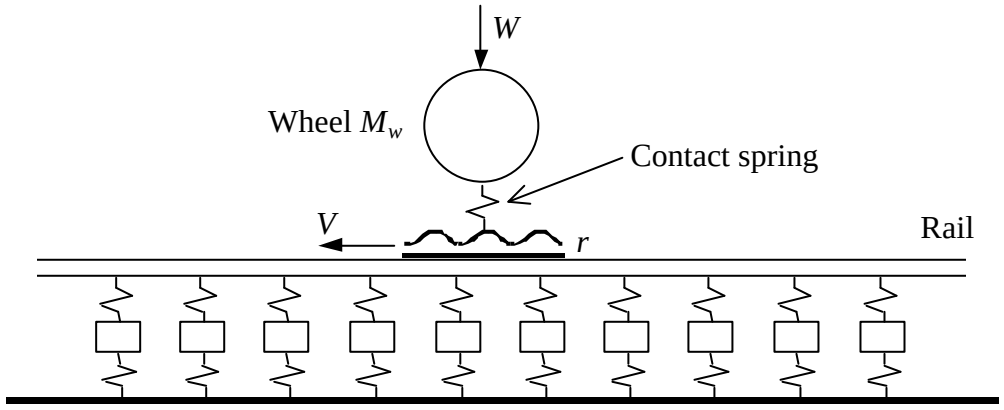

Figure 1. Representation of the excitation of the wheel/rail system by a moving irregularity.

Depending on the receptances (displacement per unit force frequency response functions) of the wheel and rail at this frequency, the roughness can result in vibration of the wheel or the rail. This vibration spreads out along the rail and around the wheel, and radiates sound. Vibration can also be absorbed by the local elasticity of

the wheel/rail contact, represented by a Hertzian contact spring. This spring has a non-linear behaviour due the geometry of the wheel/rail contact. As the compression is increased the contact area increases in size and the spring becomes stiffer. As the compression is reduced, the stiffness reduces until total unloading can occur. For contact between cylindrical bodies, the contact force F is given by [7]

$$F = \begin{cases} C_H d^{3/2}, & d = x_w - x_r - r > 0 \\ 0, & d = x_w - x_r - r \le 0 \end{cases} \tag{1}$$

where d is the deflection of the contact spring, r is the roughness relative displacement input between the wheel and rail (positive for an indentation), x_r is the rail displacement, x_w is the wheel displacement (both positive downwards) and C_H is the Hertzian constant, which depends on the radii of curvature of the surfaces and their material properties.

If the relative motion in the contact spring d varies in a small range, the above equation can be linearised by writing $F = W + dF$,

$$dF \approx \tfrac{3}{2} C_H d_0^{1/2} dd = k_H dd \tag{2}$$

where W is the nominal preload, dF is the fluctuating part of the contact force, dd is the fluctuating part of the contact deflection and k_H is the linear contact stiffness for a nominal deflection of d_0. Figure 2 shows the non-linear behaviour of equation (1) and linear approximations at two nominal preloads, 25 and 50 kN. The difference between the linear and non-linear models can be seen to be larger for a lower preload at a given relative deflection.

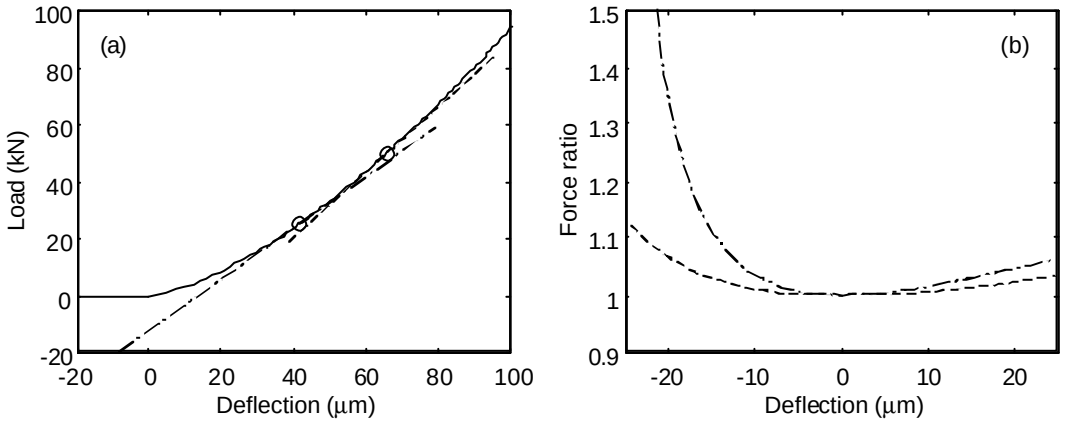

Figure 2. (a) Non-linear force-deflection relation showing linear approximations at two preloads, (b) ratios of the non-linear contact force to the equivalent linear one, - · - · static load W = 25 kN, ××××× static load W = 50 kN.

Using the linear contact stiffness of equation (2), the wheel/rail interaction model can be made linear, which allows the use of a frequency-domain approach.

This forms the basis of the model in [1]. The vibration displacement of the wheel and rail at frequency *w* are then given by

$$x_W = \frac{r a_w}{a_w + a_r + a_c}; \; x_r = \frac{-r a_r}{a_w + a_r + a_c} \tag{3}$$

where a_w is the wheel receptance at frequency *w*, a_r is the rail receptance and $a_c = 1/k_H$ is the receptance of the contact spring. Equation (3) allows for coupling in the vertical direction; actually the model in [1] includes coupling in other coordinate directions as well, in which case a matrix version of equation (3) is used [2].

2.2 Simple wheel and track models

In order to examine the effects of the approximation in equation (2), a simple model has been used in which the wheel is represented by a mass [7] or a mass and spring [8], as shown in Figure 3. Although the details of the wheel resonances at high frequencies are not included, the simple mass-spring model gives a reasonable representation of the wheel receptance up to 1 kHz, and represents the average behaviour above this.

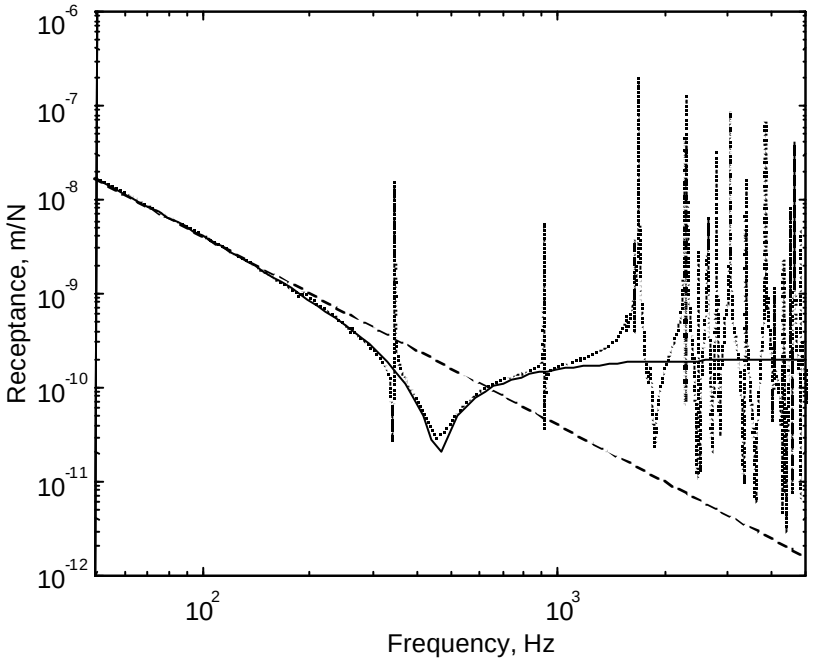

Figure 3. Wheel receptance ¾ ¾ from finite element model, ××××× from simple mass/spring model, - - - simple mass model.

The track is replaced by an equivalent state space system. This has a frequency response given by

$$H(s) = \frac{b_1 s^3 + b_2 s^2 + b_3 s + b_4}{s^4 + a_1 s^3 + a_2 s^2 + a_3 s + a_4} \tag{4}$$

where a_i and b_j are constants and $s = iw$. $H(iw)$ is the point receptance of the equivalent system. The coefficients a_i and b_j are chosen to ensure that $H(iw)$ fits closely to the receptance of a track, $a_r(w)$, modelled using a Timoshenko beam on a continuous spring-mass-spring foundation [7]. This system can also be written in the time domain as

$$(D^4 + a_1 D^3 + a_2 D^2 + a_3 D + a_4) x_r(t) = (b_1 D^3 + b_2 D^2 + b_3 D + b_4) F(t) \tag{5}$$

where D represents differential operator d/dt. $x_r(t)$ and $F(t)$ are the rail displacement and wheel/rail interaction force respectively.

The system of time-domain equations (1,5) and the corresponding equations for the wheel mass are solved using a Runge Kutta method. The results are compared with those based on using a linear contact spring, equation (2), in place of the non-linear one in equation (1). In [7,8] this has been done for a range of broad-band roughness spectra. Roughness time histories were generated from one-third octave band roughness spectra by first creating equivalent narrow-band spectra with random phase at each frequency and then applying an inverse Fourier transform. These time histories $r(t)$ were used as inputs to the wheel/rail system. From this calculation a time history of the wheel/rail interaction force was obtained. This was then transformed into the frequency domain and converted to a one-third octave force spectrum for ease of presentation.

2.3 Results

The difference between the linear and non-linear contact force spectra in one-third octave bands is shown in Figure 4 for four levels of roughness. The roughness spectra used range from a moderate roughness found on tread-braked wheels to a more severe roughness from a corrugated rail and an extreme case with twice the amplitude of the corrugated rail. The r.m.s. amplitudes of these roughnesses for the frequency range 250 Hz to 5000 Hz, r_{rms}, are 7.6, 13.2, 25 and 50 μm. Typical train speeds were used of around 100-140 km/h (at other speeds the roughness spectra would shift to different frequencies).

In each case results are shown for seven values of wheel preload, W. Typically, a passenger vehicle has a wheel load of around 50 kN, whereas that for a freight vehicle can vary between about 25 kN, when empty, and over 100 kN, when full. Preloads less than 25 kN are also included in the calculations to illustrate further the dependence on load. It is found that the linear and non-linear results are similar for low roughness amplitudes and large wheel loads, giving differences close to 0 dB, but the differences increase for large roughness and/or small loads.

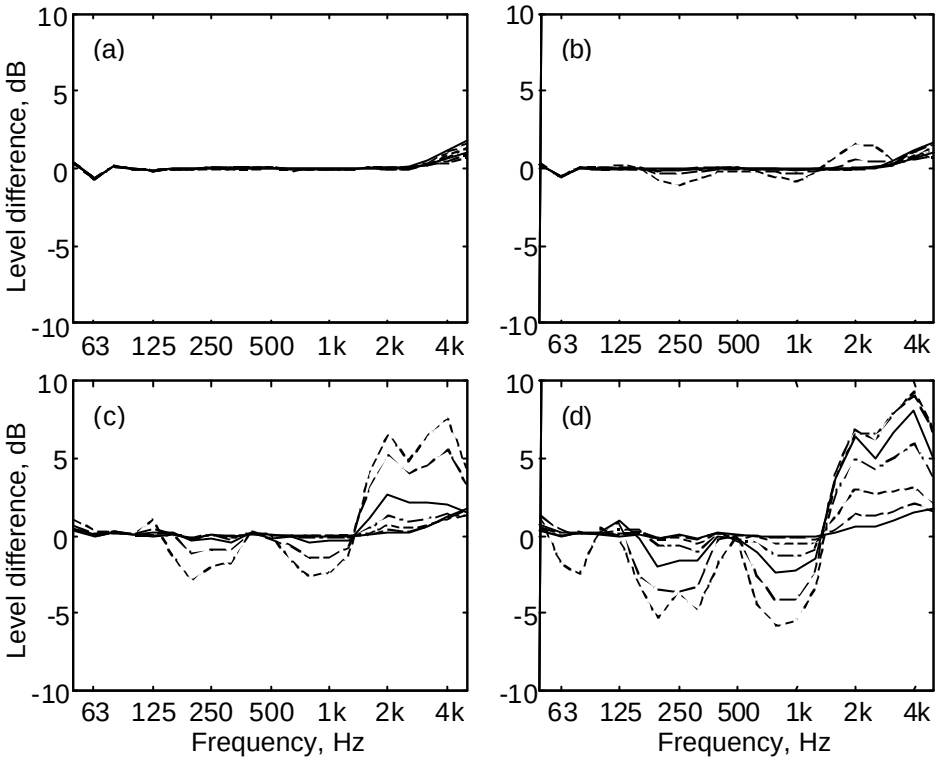

Figure 4. Difference in one-third octave band spectra of the wheel/rail contact force from the non-linear model compared to the linear model. From largest deviations to smallest, static load W = 10, 15, 25, 35, 50, 70, 100 kN. (a) moderate roughness, (b) intermediate roughness, (c) corrugated rail roughness, (d) extreme roughness.

For the tread-braked wheel roughness, r_{rms} = 7.6 μm, the two models agree very closely for all wheel loads considered. When the amplitude increases to 13 μm deviations are found for the two lowest wheel loads, although these are lower than would occur in practice. For the corrugated track roughness, the differences are small for wheel loads of 50 kN and above, but significant for loads less than that. For the extreme roughness the differences are significant for all loads except 100 kN.

As the wheel load is reduced, the static deflection of the contact spring becomes smaller, and loss of contact becomes more likely. In Figure 5(a), the average absolute difference between the results of non-linear and linear models, averaged over all frequency bands 50 to 5000 Hz, is plotted against r_{rms}/d_0, the ratio of the r.m.s. amplitude of the roughness to the static deflection of the contact spring. For all four roughness spectra considered, when this ratio is less than about 1/3 the differences are small, whereas when it is greater than about 1/2 the differences increase considerably.

In Figure 5(b), the percentage of the time over which loss of contact occurs is shown for the same cases, again plotted against the ratio r_{rms}/d_0. This shows a similar shape, although it increases from a slightly higher value of r_{rms}/d_0. This indicates that

non-linear behaviour is significant when loss of contact is occurring and just before it starts to occur, but is not significant otherwise, even though the dynamic contact force may reach peak values of two or three times the static value before loss of contact occurs.

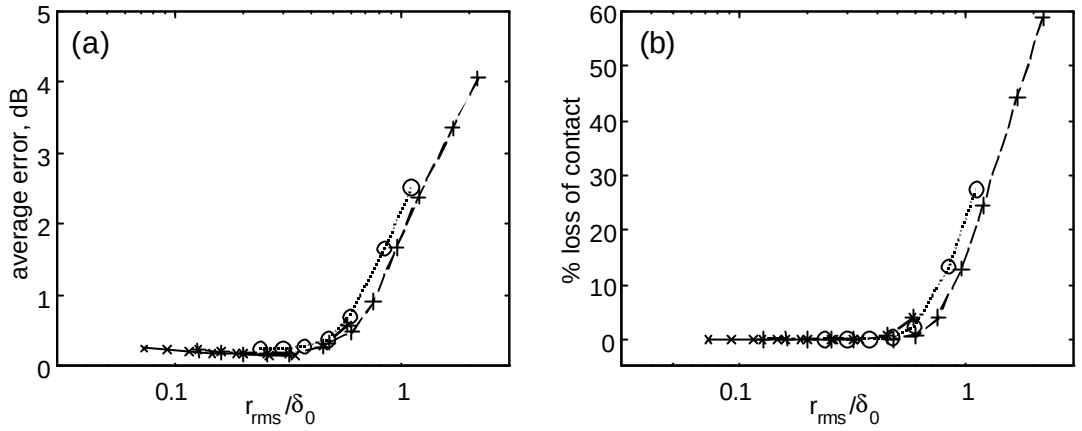

*Figure 5. (a) Average difference in one-third octave band spectra of the wheel/rail contact force from the non-linear model compared to the linear model plotted against ratio of r.m.s. roughness amplitude to static contact deflection. (b) Percentage of time that contact is fully unloaded. ´: moderate roughness, *: intermediate roughness, o: corrugated rail roughness, +: extreme roughness.*

2.4 Discussion

In ref. [7] it was shown that the non-linear effects are significant at frequencies where (i) the contact spring deflection d is a large fraction of the roughness r and (ii) the roughness itself is large. Non-linear effects can be neglected for frequencies below 100 Hz, even though the roughness inputs at these frequencies may be quite large, as the contact spring deflection d is only a small fraction of the roughness input at these frequencies. Larger effects were found for excitation around 200 and 900 Hz. These frequencies correspond to peaks in the contact force for a given roughness input. The first is due to a track anti-resonance, at which the contact stiffness and rail receptances are approximately equal and opposite. This also occurs, more strongly, at the second peak at 900 Hz. Differences can be seen at these frequencies in Figures 3(c) and (d). For frequencies above 1 kHz, although $d \approx r$ (since $|a_c| > |a_w + a_r|$ for most frequencies above 1 kHz), the roughness amplitude is generally considerably smaller than a lower frequencies. The differences seen at higher frequencies in Figure 4 are due to harmonics of the large excitation around 1 kHz on the corrugated rail.

It is concluded, therefore, that the non-linear contact spring between the wheel and the rail has only a small effect on the wheel/rail response for normal levels of surface roughness. The effects of non-linearity increase as the roughness level increases or the normal load reduces. Significant differences between the results of

linear and non-linear models occur when the r.m.s. roughness amplitude exceeds about one third of the static deflection of the contact spring. This condition corresponds closely to the onset of loss of contact, so that it is concluded that loss of contact is more important to the breakdown of the linear model than the non-linear spring stiffness. The effect on A-weighted noise levels is found to be negligible for practical situations [8]. Spectral differences greater than 1 dB are observed on a corrugated rail roughness (r.m.s. amplitude 25 μm) for wheel loads less than 50 kN, but for a roughness with r.m.s. amplitude 13 μm or less such differences do not occur for practical wheel loads. However, larger amplitude excitations occur for the wheel/rail system at discrete discontinuities such as wheel flats and rail joints. These are considered in the next sections.

3. IMPACT NOISE DUE TO WHEEL FLATS

3.1 Contact force

A wheel flat is an area of the wheel tread that has been worn flat, as shown schematically in Figure 6(a). This usually occurs due to the brakes locking up under poor adhesion conditions at the wheel/rail contact, for example due to leaves on the railhead during the autumn. Wheels with flats produce high levels of noise and impact loading of the track which can lead to damage of track components. Typically flats can be around 50 mm long, in extreme cases up to 100 mm. After their initial formation, flats become 'worn', i.e. rounded at their ends due to the high load concentration on the corners. A worn flat of a given depth is longer than the corresponding 'new' flat.

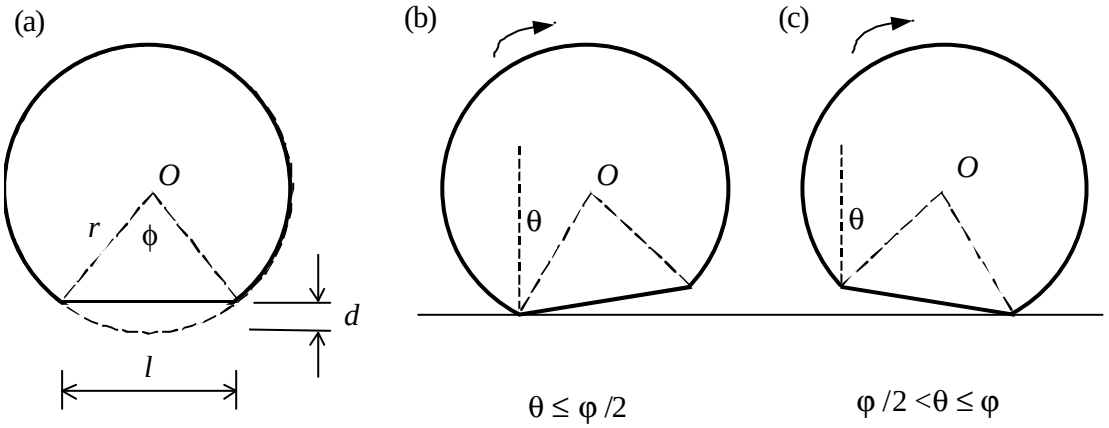

Figure 6. Rolling of a wheel with an idealised flat.

Wheel flats introduce a relative displacement input to the wheel/rail system in the same way as roughness. The profile shape can be seen to correspond to a circular arc dip in the railhead. However, due to the geometry of the wheel and rail surfaces,

the actual displacement input is modified by the wheel curvature. For the idealised flat shown in Figure 6(a), the wheel first pivots downwards on the front corner of the flat, Figure 6(b), then pivots upwards again on the rear corner [9], Figure 6(c). The resulting relative displacement input experienced by the wheel/rail system is shown in Figure 7. In ref. [9] it is shown that a worn wheel flat can be represented by a curve of a similar shape to that in Figure 7 but elongated.

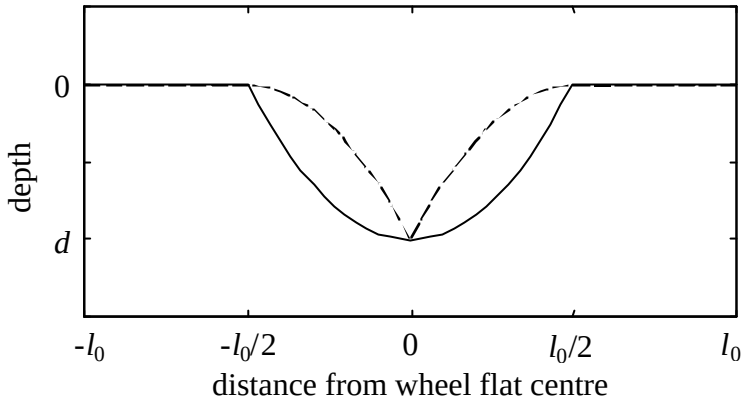

Figure 7. Wheel flat geometry for new flat of length l_0 and depth d. - - - - profile shape, - - - after geometric filtering.

The response of the wheel and rail can be calculated using the same model as described in the previous section. In ref. [9] the wheel is represented by a mass and a spring (see Figure 3). For numerical convenience an additional small mass is attached on the underside of the spring. Figure 8 shows examples of the calculated response to a new wheel flat of depth 2 mm (length 86 mm). The contact force has a static value of 100 kN.

When the indentation (relative displacement input due to the wheel flat) appears between the wheel and rail, the wheel falls and the rail rises. Since the wheel and rail cannot immediately follow the indentation due to their inertia, the contact force is therefore partly unloaded. At a train speed of 30 km/h, Figure 8(a), full unloading first occurs.

After the relative displacement input reaches its maximum, the contact force increases rapidly until it reaches its peak (the wheel is now pivoting about the trailing edge of the flat). The peak force is here about 4 times as large as the static load. As the speed increases, contact is lost for longer during the unloading phase. At 80 km/h, Figure 8(b), a second loss of contact can be seen to occur. At the first impact at about 3.5 ms the force rises dramatically. Since the momentum of the wheel and rail are changed dramatically by the large impulse during this first impact, the wheel and rail are forced to move apart from each other and a second loss of contact occurs at about 7.5 ms. However, the second impact is much smaller than the first one. For a rounded flat of the same depth but overall length 121 mm the speed at which loss of contact first occurs increases from 30 km/h to about 50 km/h.

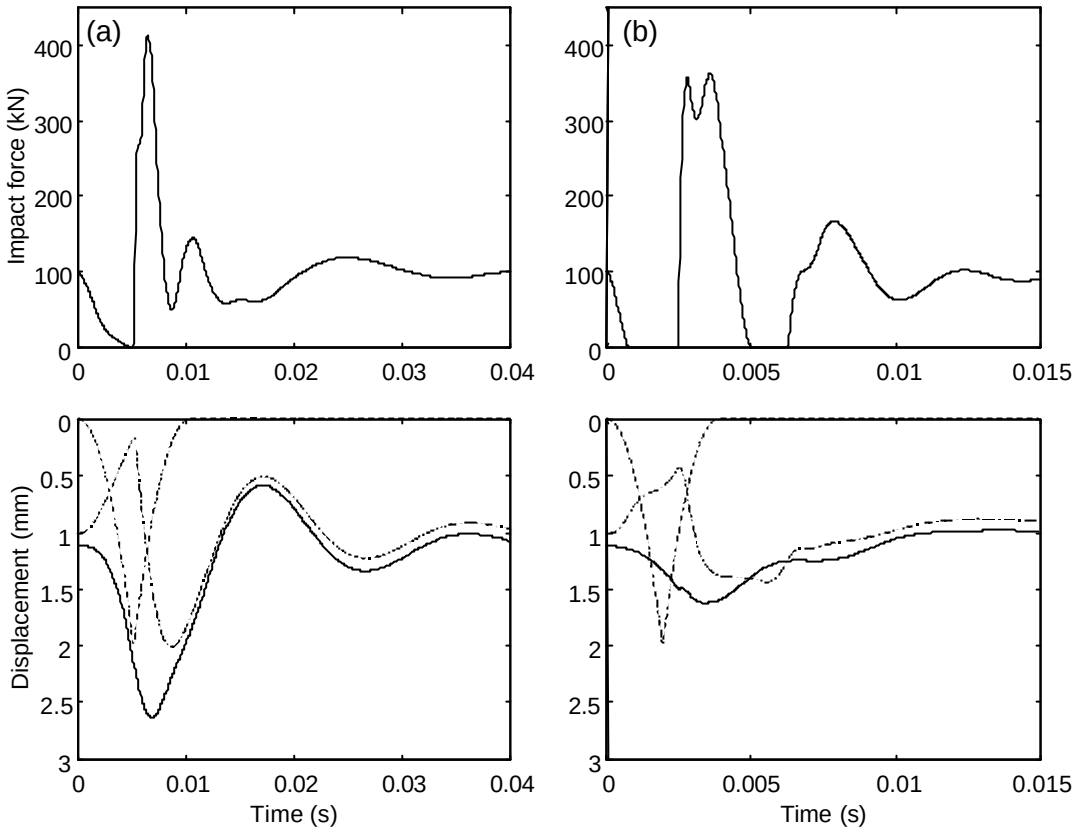

Figure 8. Wheel/rail interaction and displacements of wheel and rail due to 2 mm newly formed wheel flat. (a) At train speed 30 km/h, (b) at 80 km/h, ¾ ¾ wheel displacement, - ˙ - ˙ rail displacement, ˙˙˙˙˙ relative displacement excitation.

The maximum contact force is plotted against train speed in Figure 9 for several cases. The details of the contact force depend on the flat geometry. Comparisons with measured impact forces [10] suggest that the geometrical effect of wheel curvature indicated in Figure 7 leads to over-estimates of the contact force. In future work it is planned to use measured wheel flat profiles to study this effect further.

3.2 Noise prediction

The above process is sufficient to estimate the contact forces, including the effects of contact non-linearity. The next stage is to use these results to estimate the radiated noise. For this, the response of the wheel and rail are required incorporating details of the wheel modes of vibration and the propagation of vibration along the rail. Such effects are included in the conventional rolling noise model, TWINS [1].

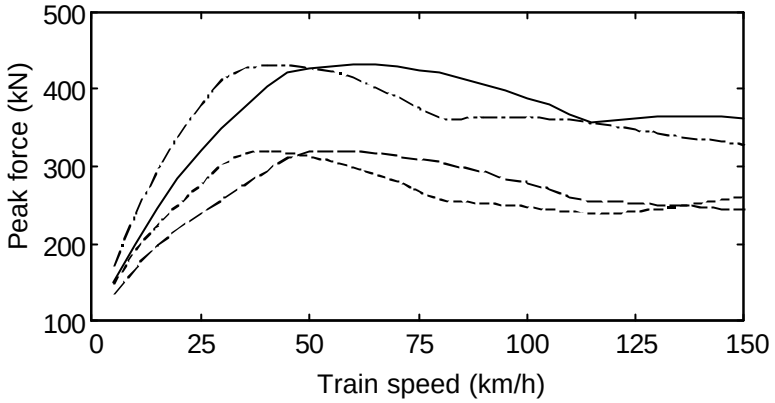

Figure 9. Peak impact force predicted from different wheel flats. ¾ ¾ due to 2 mm rounded flat, - - - 1 mm rounded flat, - ¥ - ¥ 2 mm newly formed flat, ¥¥¥¥¥ 1 mm newly formed flat.

Unfortunately, it is not possible to use the contact force obtained from the impact model and apply it directly within the TWINS model, because the interaction force is sensitive to details of the wheel and track dynamics. With a modal wheel model, the force will have strong dips at the wheel resonance frequencies. The wheel response has only shallow peaks, just above the resonance frequencies, the interaction with the track thereby introducing apparent damping to the wheel [3].

A hybrid approach has therefore been developed in ref. [9] whereby an equivalent roughness spectrum is derived. This is defined such that the contact force spectrum obtained using the above *non-linear* model is identical to that obtained using a *linear* model excited by the equivalent roughness spectrum. At this stage the wheel and track are represented by the same simple elements described above in both cases. The equivalent roughness spectrum can then be used as the input to a more detailed linear frequency-domain model, such as the TWINS model, to predict the noise due to the impact. This procedure has been validated in [9].

Example results are given in Figure 10(a). This shows the sound power due to one wheel and the associated track vibration for a 2 mm new wheel flat at different speeds for 100 kN wheel load. Results correspond to the average over a whole wheel revolution. Figure 10(b) shows, for comparison, corresponding results for roughness excitation due to the moderate roughness considered in Section 2 (tread-braked wheel roughness). The wheel is represented by its full modal basis in the frequency range up to 6 kHz, determined from a finite element model. The track is modelled by a Timoshenko beam, continuously supported on layers of damped springs and mass. As the speed increases, the noise at frequencies above about 200 – 400 Hz increases in both cases. The increase in rolling noise with increasing speed is greater than that due to the flat. For the wheel flats that were considered here, the noise generated exceeds that due to the tread-braked wheel roughness at all speeds and in all frequency bands, although the noise due to roughness increases more rapidly with speed so that at

sufficiently higher speeds it can be expected to dominate. For corrugated track, the noise due to roughness exceeds that due to wheel flats at 120 km/h.

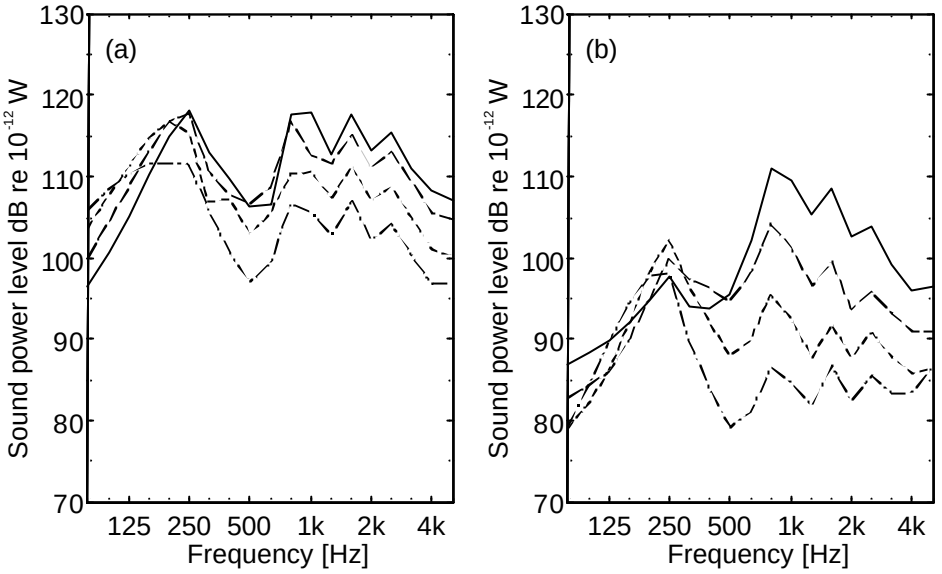

Figure 10. Sound power level due to wheel and track. (a) 2 mm new wheel flat, (b) rolling noise from moderate roughness. - x - x 30 km/h, xxxxxx 50 km/h, - - - 80 km/h, ¾ ¾ 120 km/h.

Figure 11 shows a summary of the variation of the overall A-weighted sound power level with train speed. The predicted noise level due to conventional roughness excitation increases at a rate of approximately 30 $\log_{10}$ V, where V is the train speed, whereas the noise due to flats increases at an average of around 20 $\log_{10}$ V onve loss of contact occurs For example, loss of contact was found to occur for the newly formed 2 mm flat at speeds above 30 km/h and for the rounded 2 mm flat above 50 km/h. This variation with speed indicates that the radiated sound due to wheel flats continues to increase with increasing speed, even though loss of contact is occurring.

Impact noise from wheel flats is found to depend on the wheel load. The increase in noise between a load of 50 kN and 100 kN is about 3 dB. In contrast, the rolling noise due to roughness is relatively insensitive to wheel load.

4. IMPACT NOISE DUE TO RAIL JOINTS

In a similar way to wheel flats, rail joints provide discrete inputs to the wheel/rail system that induce quite large contact force variations. Rail joints can be characterised by a gap width and a step height (either up or down). Moreover, the rail often dips down to a joint on both sides. Such dips are also present at welds, and are usually characterised in terms of the angle at the joint.

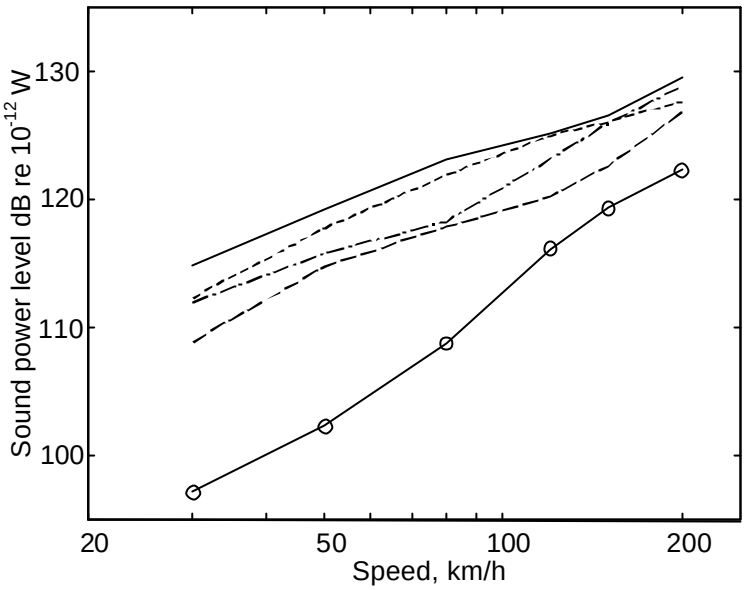

Figure 11. Sound power radiated by one wheel and the associated track vibration. - - - 1 mm rounded flat, xxxxxxx 2 mm rounded flat, - x - x 1 mm new flat, ¾ ¾ 2 mm new flat, o - - - o *rolling noise due to roughness (moderate roughness).*

A similar approach has been used as above to study the effects of rail joints [11,12]. To allow for the reduced bending stiffness at a fish-plated joint a model of a pin-jointed beam was adopted [11]. The sound radiation was calculated using the same hybrid method as for the wheel flats, except that a correction had to be introduced to allow for the pin-jointed model of the rail receptance. It was found, for realistic parameter values, that the gap width is insignificant compared with the step height and dip angle and this will not be considered further here.

Results are shown in Figure 12(a) for un-dipped rail joints in the form of the total A-weighted sound power emitted by the wheel and rail during 1/8 sec. The results for a step-down joint are found to be virtually independent of the step height (only results for one value are shown) and also change very little with train speed. The same is found to be the case for the peak contact force [1]. However, for step-up joints both the peak contact force and the sound power level increase with step height and with train speed. The sound power level from a single joint has a speed dependence of around 20 $\log_{10}V$.

In Figure 12(b) results are given for dipped joints with no height difference. Here a dip of 5 or 10 mm is considered as a quadratic function over a length of 0.5 m either side of the joint. A dip of 5 mm corresponds to a joint angle of 0.04 radians which is large although typical, a dip of 10 mm corresponds to 0.08 radians which is severe. The 10 mm dip produces a similar noise level to a 1 mm step-up un-dipped joint, although for speeds above 120 km/h the noise level from the dip joint becomes independent of train speed.

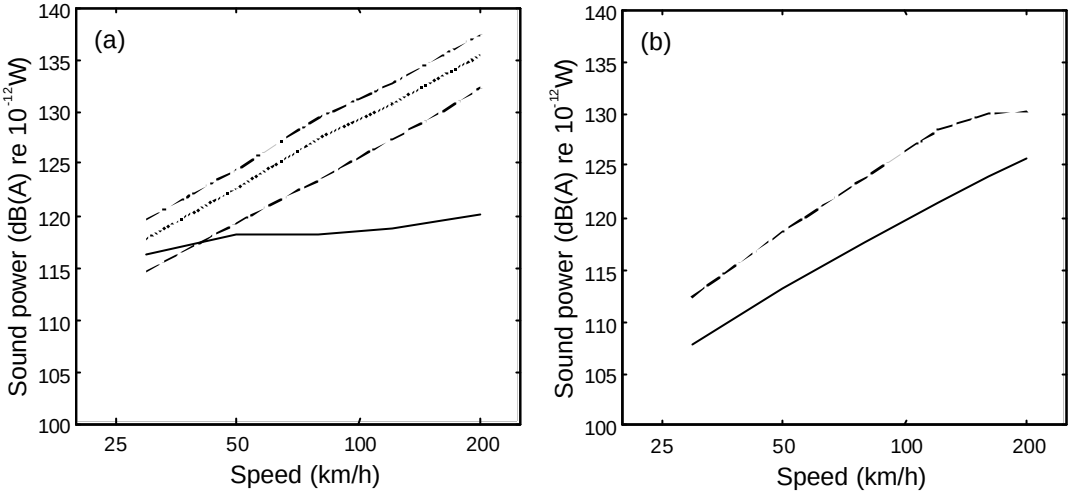

Figure 12. A-weighted sound radiated by one wheel and the associated track vibration during 0.125 second due to a wheel passing over (a) flat rail joints, - - - 1mm step-up, xxxxxx 2 mm step-up, x -x - 3 mm step-up, ¾ ¾ 2 mm step-down (b) dipped rail joints with no height difference, ¾ ¾ 5 mm dip, - - - 10 mm dip (all with 7 mm gap).

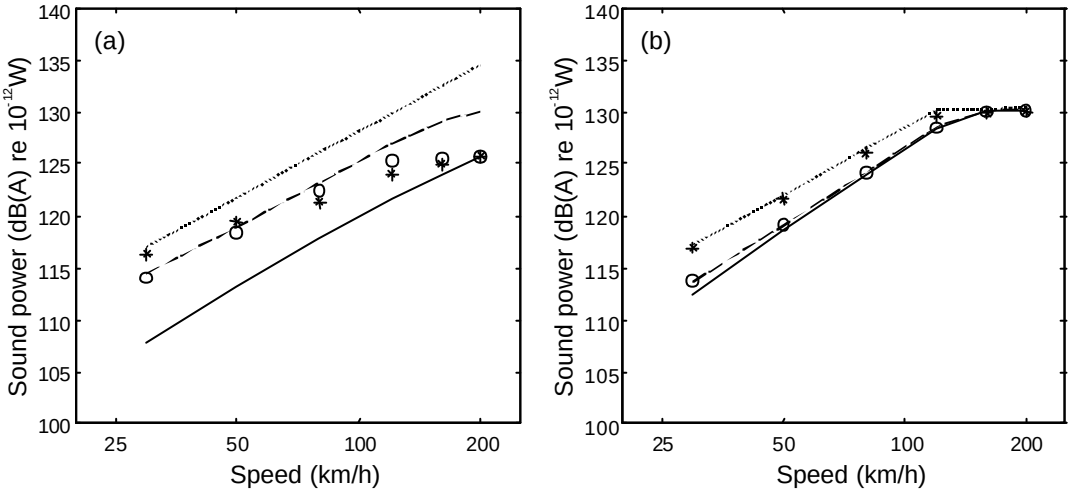

*Figure 13. A-weighted sound power radiated by one wheel and the associated track vibration during 0.125 second due to a wheel passing over different rail joints with 7 mm gap and 5 or 10 mm dip. (a) for 5 mm dip, (b) for 10 mm dip. xxxxxx 2 mm step-up, - - - 1 mm step-up, ¾ no height difference, * 2 mm step-down,* o *1 mm step-down.*

Figure 13 shows the predicted noise for joints with both dipped rails and steps. The noise radiation generally increases with speed, regardless of whether loss of contact occurs. For the 5 mm dip, the noise level increases by 8 dB when the step height increases from 0 to 2 mm. For the step-down joints, the noise level is higher

than without a step, although at higher speeds the dip has more effect than the step. The results for the 10 mm dip are similar for both step-up and step-down joints indicating the dominance of the dip in this case.

These results may be compared with the rolling noise results given in Figure 11 and are seen to be 5-20 dB greater. However, this comparison is related to the sound within 1/8 sec. indicating that the joint can be heard above the rolling noise. To evaluate their effect on the average noise level, the time base of the joint noise should be adjusted to the average time between joints. This shows [11] that rolling noise due to the moderate roughness considered above is similar to the average noise due to 5 mm dipped joints with no height difference. With a height difference of 2 mm the average noise predicted from the joints increases to almost 10 dB greater than the rolling noise. Moreover, since the time between rail joints decreases as train speed increases, it is also found that the average noise level from joints increases at about 30 $\log_{10}$V, similar to rolling noise.

5. EFFECTS OF WHEEL MODES OF VIBRATION

It is known from studies of rolling noise that the wheel modes containing a significant radial component of motion at the contact zone dominate the noise radiation at frequencies above about 1.5 to 2 kHz [13]. High frequency wheel modes have been neglected in calculating the interaction force in the previous sections, but have been accounted for in the hybrid approach used to predict the noise. To investigate the effect of these wheel modes, they are included in the non-linear model in this section for an example case.

The radial point receptance of a wheel at the contact point can be given in terms of a modal summation over N modes as

$$a_w = \sum_{n=1}^{N} \frac{y_n^2}{w_n^2 - w^2 + 2iz_n w_n w} \tag{6}$$

where, for the nth mode, y_n is the mass-normalised modeshape at the contact point, w_n is the natural frequency and z_n is the damping ratio. The net downwards force applied to the wheel is $W - F(t)$ where W is the static wheel load. In the time domain, the modal amplitude $y_n(t)$ of each mode satisfies a single degree-of-freedom equation

$$\ddot{y}_n + 2z_n w_n \dot{y}_n + w_n^2 y_n = y_n (W - F), \quad n = 1, 2, \ldots, N \tag{7}$$

The wheel displacement at the contact zone is composed of a superposition of all the modal displacements, y_n

$$x_w(t) = \sum_{n=1}^{N} y_n(t) y_n, \quad n = 1, 2, \ldots, N \tag{8}$$

Equation (7) can be expressed in state space form using the state variables y_n and $\dot{y}_n$ and solved using a Runge Kutta method along with equations (1) and (5). The

only difficulties are that there is a considerable increase in the number of state variables and that the modal damping is low.

Results are given for a single case of a 5 mm dipped joint with a 1 mm step-up, as in Section 4. The wheel speed is 80 km/h and the static load 100 kN. The wheel is represented by 12 flexible modes (radial and one-nodal circle) as well as by its mass (rigid-body mode). These modes are sufficient to represent the receptance in the radial direction for frequencies up to about 5 kHz.

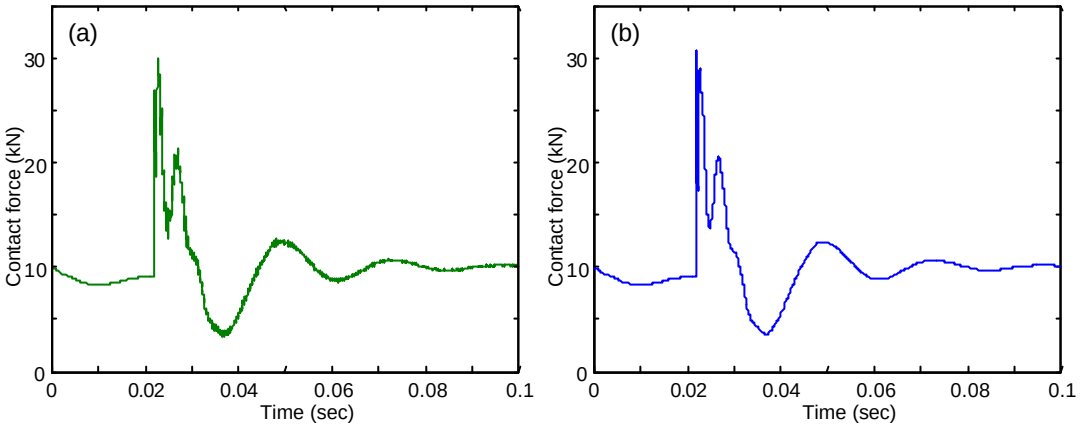

Figure 14. Wheel/rail impact forces for a dipped rail joint at 80 km/h (a) calculated using a modal wheel, (b) calculated using a mass wheel.

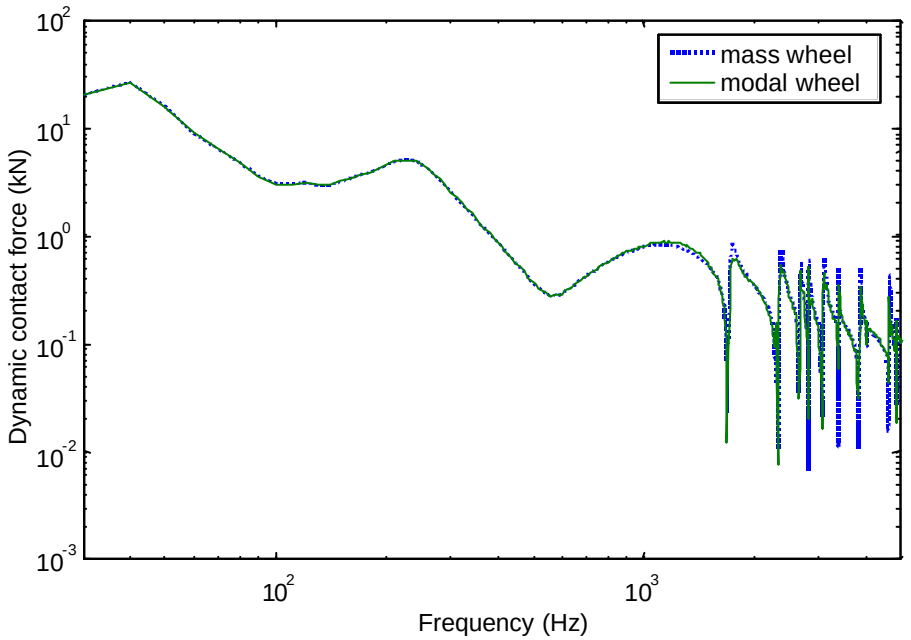

Figure 15. Wheel/rail impact force spectra for a dipped rail joint at 80 km/h ¾ calculated using a modal wheel, - - - calculated using a mass wheel, corrected using hybrid approach.

Figure 14 shows the contact force results in the time domain for this and for a simple mass. The results are very similar, although with the modal wheel high frequency oscillations are present. Figure 15 shows the force spectra. In the case of the simple wheel, these have been corrected using the procedure described in Section 3. The corresponding results show very good agreement.

6. CONTACT FILTER EFFECTS

The wheel/rail contact exists over an area typically 10-15 mm long. When excited by roughness with wavelengths shorter than this length, the excitation is attenuated compared with that at longer wavelengths. This effect is known as the 'contact filter' [14]. Such a filtering effect can be applied to random roughness excitation as a frequency-domain correction. In fact, in the analysis described in Section 2, the roughness spectra used to generate the inputs were already filtered. Such filters have been based on analytical formulae [15] or on the results of numerical simulations using a 'Discrete Point Reacting Spring' (DPRS) model with actual roughness data [16].

However, for excitation by wheel flats or rail joints a time-domain approach to implementing the contact filter is required. The results given in Sections 3 and 4 do not take any account of contact filtering. Introducing a contact filter will attenuate high frequency components of vibration and noise. For the above results this will lead to reductions in the predicted sound power above about 1 kHz at 160 km/h, correspondingly lower frequencies at lower speeds.

During impact, the contact spring deflection varies considerably and consequently the contact patch length varies. As a result, a simple frequency domain filter is no longer appropriate. To overcome this a method based on a two-dimensional version of the DPRS model has been developed. The wheel/rail contact is replaced by a 'mattress' of springs distributed over the contact zone. The stiffness of these springs is chosen such that together they replicate the three-dimensional Hertzian contact stiffness – whereas in the three-dimensional DPRS model their stiffness has to be non-linear this is not necessary for a two-dimensional mattress model. However, as in the three-dimensional DPRS model, the radii of curvature of the wheel and rail have to be modified to ensure the correct contact patch length is simulated for a given normal load. Validation of the results of this approach has been provided by an 'exact' Boussinesq model [16,17].

Figure 16 shows some results obtained using various different contact filter models. The results using the DPRS model are obtained as the average of the results obtained using this model in combination with six different sets of wheel roughness data [14]. The results of the analytical contact filter, from [15], can be seen to give too great an attenuation at high frequencies. The two-dimensional mattress model gives slightly too little attenuation here but its results are quite encouraging. Such a simple mattress model can readily be incorporated into the simulations of impact due to wheel flats and rail joints although this has not yet been done.

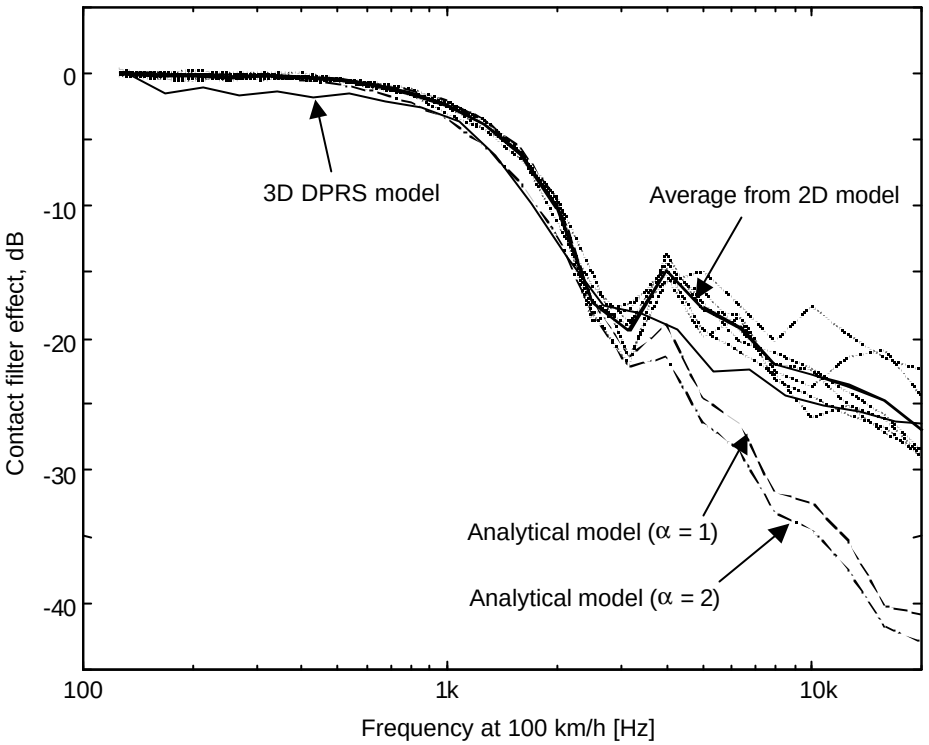

Figure 16. Contact filter effect, - - - analytical model a = 1, ᵡ-ᵡ- analytical model a = 2, ᵡᵡᵡᵡᵡ results from 2D mattress model for six sets of wheel roughness data, ▬▬ average 2D result, ¾ average result from 3D DPRS model.

7. CONCLUDING REMARKS

This paper has reviewed recent work on the effect of non-linearities in the contact zone on the excitation of wheel/rail noise. It has been shown that, for rolling noise due to roughness excitation, non-linearities play a negligible role, whereas for discrete discontinuities such as wheel flats and rail joints, the effects of non-linearities should be taken into account. A hybrid approach has been developed allowing the non-linear wheel/rail interaction to be calculated using simple but representative wheel and track models and converting the results back to an equivalent roughness that can be used with a linear frequency-domain model to predict noise.

A 1/5 scale model rig has been used for experimental validation of the results of impact noise generation. Tests have been carried out using a simulated wheel flat (in the rail head), dipped joints and stepped joints as well as a relatively smooth rail. A range of preloads and wheel speeds have been used. Initial results are promising, although analysis has not yet been completed [18].

A number of other aspects of wheel/rail interaction have been studied and will be mentioned only briefly to conclude. The modelling described here has been based on interaction in only the vertical direction. Inclusion of the lateral coordinate as well has been considered in [19]. For this the track had to be represented by a similar

model to that given by equation (4) for both the lateral and cross receptances using higher order polynomials. The wheel and rail are coupled in the lateral direction by a creep force which is sensitive to the normal load, so that if loss of contact occurs this force also becomes zero. The vertical interaction is found to be largely unaffected by the addition of lateral coupling, although the lateral response is only correctly predicted when the lateral coupling is included.

Roughness growth on the wheel and rail surface is affected by wheel/rail dynamics as well as wear phenomena. It has been found that rail roughness growth is influenced by the presence of multiple wheels on the rail [20,21]. Waves in the rail are reflected by neighbouring wheels, leading to fluctuations with frequency in the point receptance of the track and, as a result, the contact force. These lead to roughness growth at frequencies associated with peaks in the contact force that have a particular phase angle relative to the roughness excitation [21].

For a discretely supported track, the time-varying dynamic stiffness that is experienced by the wheel can induce parametric excitation. It has been possible to use a track model similar to that of equations (4,5) but with time-varying coefficients to estimate the effect of parametric excitation [22]. For this, a discretely supported track had to be used as the basis for choosing the constants a_i and b_j, and an eighth order model was used in place of the fourth order one presented in Section 2. This study has shown that, while there is a large component at the sleeper-passing frequency and its first few harmonics, the amplitude at higher frequencies is generally less than that due to roughness excitation. Nevertheless, if roughness can be reduced, parametric excitation will present a lower limit to the noise that is produced by the wheel/rail system, which can only be overcome by using a continuous track support.

ACKNOWLEDGEMENT

The work described has been carried out within the project 'Non-linear Effects at the Wheel/rail Interface and their Influence on Noise Generation' funded by EPSRC (Engineering and Physical Sciences Research Council of the United Kingdom), grant GR/M82455.

REFERENCES

1. D.J. Thompson, B. Hemsworth, N. Vincent, "Experimental validation of the TWINS prediction program for rolling noise, part 1: description of the model and method". *J. Sound Vib.* **193**, 123-135 (1996).
2. D.J. Thompson, "Wheel-rail noise generation, part I: introduction and interaction model", *J. Sound Vib.* **161**, 387-400 (1993).
3. D.J. Thompson, "Wheel-rail noise generation, Part IV: contact zone and results", *J. Sound Vib.* **161**, 447-466 (1993).
4. T.X. Wu, D.J. Thompson, "Effects of local preload on the foundation stiffness and vertical vibration of railway track", *J. Sound Vib.* **219**, 881-904 (1999).

5. R.A. Clark, P.A. Dean, J.A. Elkins, S.G. Newton, "An investigation into the dynamic effects of railway vehicles running on corrugated rails", *J. Mech. Eng. Sci.* **24**, 65-76 (1982).
6. J.C.O. Nielson, A. Igeland, "Vertical dynamic interaction between train and track – influence of wheel and track imperfections", *J. Sound Vib.* **187**, 825-839 (1995).
7. T.X. Wu, D.J. Thompson, "Theoretical investigation of wheel/rail non-linear interaction due to roughness excitation". *Veh. Syst. Dyn.* **34**, 261-282 (2000).
8. D.J. Thompson, T.X. Wu, "The effects of non-linearities at the wheel/rail interface on the generation of rolling noise". *Proc. Internoise 2001* The Hague, Holland, 129-134 (2001).
9. T.X. Wu, D.J. Thompson, "A hybrid model for the noise generation due to railway wheel flats". *J. Sound Vib.* **251**(1), 115-139 (2002).
10. A. Johansson, J. Nielsen, "Railway wheel out-of-roundness – influence on wheel-rail contact forces and track response", Proc. Wheelset Congress, Rome (2001).
11. T.X. Wu, D.J. Thompson, "On the impact noise generation due to a wheel passing over rail joints". *Proc. 7th Int. Workshop on Railway Noise*, Portland, Maine, USA (2001).
12. T.X. Wu, D.J. Thompson, "A model for impact forces and noise generation due to wheel and rail discontinuities". *Proc. 8th Int. Congress Sound and Vib.*, Hong Kong, China, 2905-2912 (2001).
13. D.J. Thompson, "Wheel-rail noise generation, part II: wheel vibration", *J. Sound Vib.* **161**, 401-419 (1993).
14. D.J. Thompson, "The influence of the contact zone on the excitation of wheel/rail noise". *Proc. 7th Int. Workshop on Railway Noise*, Portland, Maine, USA (2001).
15. P.J. Remington "Wheel/rail rolling noise, I: Theoretical analysis". *J. Acoust. Soc. Am.* **81**, 1805-1823 (1987).
16. P.J. Remington, J. Webb "Estimation of wheel/rail interaction forces in the contact area due to roughness". *J. Sound Vib.* **193**, 83-102 (1996).
17. R. Ford, D.J. Thompson, 2003 "Contact filters in wheel/rail noise prediction". *ISVR Technical Memorandum* in preparation (2003).
18. T.D. Armstrong, "Use of a scale model rig to investigate non-linear wheel/rail interaction". PhD thesis, University of Southampton, in preparation (2003)
19. T.X. Wu, D.J. Thompson, "Wheel/rail non-linear interaction with coupling between vertical and lateral directions". Accepted for publication, *Veh. Syst. Dyn.* (2003).
20. T.X. Wu, D.J. Thompson, "Behaviour of the normal contact force under multiple wheel/rail interaction". *Veh. Syst. Dyn.* **37**, 157-174 (2002).
21. T.X. Wu, D.J. Thompson, "An investigation into rail corrugation due to micro-slip under multiple wheel/rail interactions". *Proc. 6th Int. Conf. on Contact Mechanics and Wear of Wheel/Rail Systems*, Gothenburg (2003).
22. T.X. Wu, D.J. Thompson, "On the parametric excitation of the wheel/track system". Submitted to *J. Sound Vib.* (2003)